JOURNAL OF CATALYSIS **159,** 150–161 (1996)
ARTICLE NO. 0074

Surface and Catalytic Properties of Lanthanum-Promoted Ni/Sepiolite Catalysts for Styrene Hydrogenation

S. Damyanova,* L. Daza,† and J. L. G. Fierro[1,†]

*Institute of Kinetics and Catalysis, Bulgarian Academy of Sciences, 1113 Sofia, Bulgaria; and †Instituto de Catálisis y Petroleoquímica, CSIC, Campus UAM, Cantoblanco, 28049 Madrid, Spain

Received November 1, 1994; revised October 2, 1995

The catalytic behavior for styrene hydrogenation of two series of La-promoted nickel/sepiolite catalysts (*x*LaNi and Ni*x*La) is reported. Both series were prepared by two-step impregnations, but lanthanum was incorporated first and nickel afterward in Ni*x*La series and the order was reversed in *x*LaNi samples. The catalysts were characterized by temperature-programmed reduction (TPR), kinetics of reduction by hydrogen, photoelectron spectroscopy (XPS), and infrared spectroscopy of adsorbed CO to obtain information on the nature and distribution of nickel and lanthanum in the oxidic and reduced samples. The kinetics of reduction and XPS data indicate clearly that Ni^{2+} ions interact strongly with the sepiolite substrate in *x*LaNi samples and to a lesser extent in Ni*x*La series. The IR spectra of CO adsorbed on the reduced catalysts demonstrate that the promotion of Ni/sepiolite catalyst with lanthana results in a change in the distribution of CO-adsorbed structures. It appears that reconstruction of bridge-bonded species occurs via formation of Ni(100) surfaces. Moreover, CO can be adsorbed in a linear form on Ni atoms which are in contact with oxidic phase. The decrease of the bridged form and relative higher concentration of unreduced nickel species gives an indication that lanthanum is deposited on the nickel particles, leading to a decrease in the probability to have adjacent nickel atoms on the surface. The observed stable maximum in activity for the Ni7.1La catalyst is caused not only by covering by La a larger fraction of the silicate substrate but also by isolating Ni atoms on the surface of Ni crystallites by La_2O_3 patches deposited on it.

INTRODUCTION

Supported nickel catalysts have been used usually for hydrogenation reactions. Several recent studies (1–7) have shown that the specific activity and selectivity of the nickel catalysts strongly depend on the promoters and type of supported metal. Rare-earth oxides have been used often as promoters in hydrogenation catalysts. The surface properties of these additives have attracted a growing interest from the point of view of heterogeneous catalysis because the lanthanide transition-metal compounds exhibit catalytic activities higher than those of commercial Ni catalysts. It has been reported that the incorporation of lanthanum oxide modifies to a great extent the chemical and physical characteristics of the support and of supported metal oxides. Addition of lanthanum oxide to nickel-alumina catalysts increases the thermostability of the catalysts (8–10). Schaper *et al.* (10) have suggested that the nucleation of $LaAlO_3$ on the surface hinders the phase transition from γ-alumina to α-alumina. Using X-ray diffraction (XRD), Raman spectroscopy, and X-ray photoelectron spectroscopy (XPS), Ledford *et al.* (11) have demonstrated that lanthanum inhibits the sintering of γ-alumina and acts as a dispersant for the added metals.

The work presented in this study is a continuation of the studies performed in our laboratory on sepiolite-supported nickel catalysts (12, 13) and compiles data related to the effect of lanthanum on the structure and reactivity of these catalysts. XPS, TPR, XRD, FTIR spectroscopy of CO adsorption, and kinetics of reduction were used to reveal the influence of the promoter on the state and dispersion of nickel on the sepiolite substrate. The surface and bulk properties of the catalysts are discussed within the framework of their catalytic performance in the reaction of styrene hydrogenation.

EXPERIMENTAL

Catalyst Preparation

Two series of sepiolite-supported La-promoted nickel catalysts were prepared. The sepiolite support from Yunclillos, Toledo (Spain) was provided by Tolsa, S. A. Its chemical analysis was: SiO_2, 66.19%; MgO,13.16%; Na_2O, 1.71%; Al_2O_3, 1.66%; CaO, 0.66%; K_2O, 0.41%; and Fe_2O_3, 0.36%. The first catalyst series was prepared by incipient wetness impregnation of the support with aqueous solutions of nickel nitrate (Merck, reagent grade). The samples were subsequently dried at 383 K for 15 h and reduced at 673 K for 2 h in hydrogen flow. Both the sepiolite substrate and the reduced Ni samples were impregnated with solutions

[1] To whom correspondence should be addressed.

0021-9517/96 $18.00

containing the requisite amount of lanthanum nitrate hexahydrate (Merck, reagent grade) followed by drying and calcination at 723 K for 2 h, while the bimetallic catalysts were then reduced at 673 K for 2 h. The second catalyst series was prepared by impregnation of La-modified support with aqueous solution containing the required amount of nickel nitrate. Then the samples were dried, calcined, and reduced as above.

The nickel content for both catalyst series ranged between 4.3 and 5.3 wt% and the La content was in the range 2.3–8.7%. The samples are referred to hereafter as *x*La for La-modified supports, *x*LaNi for the first catalyst series, and Ni*x*La for the second one, where *x* denotes the La percentage of the catalysts.

Methods of Catalyst Characterization

The nickel and lanthanum content of the catalysts was determined using a Perkin–Elmer 3030 atomic absorption spectrophotometer, following acid digestion of the samples. The surface area was calculated by the BET from the nitrogen adsorption isotherms taking a value of 0.162 nm^2 for the cross section of the adsorbed N_2 molecule. These isotherms were measured in an automatic Micromeritics ASAP 2000 apparatus selecting only the range of relative pressures $0.05 \leq P/P_0 \leq 0.30$ for BET calculation. Powder X-ray diffraction measurements were obtained at room temperature with a Rigaku diffractometer. Nickel filtered Cu$K\alpha$ radiation was used and a scan speed of 2° min^{-1} was fixed in all experiments.

Kinetic curves of reduction were recorded with a Cahn 2000 microbalance working at a sensitivity of 1 μg. For reducibility runs, a 100-mg calcined sample was heated in a flow (50 ml min^{-1}) of air 5% vol in helium at 773 K up to constant weight to remove adsorbed water and other gaseous contaminants, then cooled at room temperature in pure helium (50 ml min^{-1}). Subsequently, the flow was switched to a gas mixture (50 ml min^{-1}) consisting of 10% vol H_2 (99.995% vol) in helium and increasing temperature at a rate of 4 K min^{-1} up to 673 K while continuously recording the weight changes. The weight loss recorded was taken as a measure of the extent of reduction. The microbalance was interfaced with a microcomputer for data acquisition and processing. The nickel degree of reduction was defined by the ratio $\alpha = \Delta W_t/\Delta W_{eq}$, where ΔW_t and ΔW_{eq} are the weight change at a given time and equilibrium, respectively.

Temperature-programmed reduction (TPR) experiments were carried out in an automatic Micromeritics 3000 equipment interfaced to a data station. Since water is produced during reduction, the gas exiting from the reactor was passed through a cold trap before entering the thermal conductivity detector. Calcined sample (30 mg) was heated at 4 K min^{-1} from 290 K to 1070 K in 50 ml min^{-1} of 10% H_2/He mixture.

Infrared spectra of adsorbed CO on reduced catalysts were recorded on a Nicolet 5ZDX spectrometer at a resolution of 4 cm^{-1} and were averaged over 100 scans. The prereduced samples in the form of self-supporting wafers of 10 mg cm^{-2} were evacuated at 723 K for 1 h within a special infrared cell fitted with greaseless stopcocks and KBr windows. The specimens were reduced *in situ* in a hydrogen flow (60 ml min^{-1}) at 673 K for 1 h. After reduction, the catalysts were outgassed for 30 min at the same temperature, cooled to room temperature, and then exposed to CO. The net spectra were obtained by subtracting the background of sample from the whole spectra.

Photoelectron spectra were recorded on a Fisons ESCALAB 200R electron spectrometer using Mg$K\alpha$ radiation (Mg$K\alpha = 1253.6$ eV) and a hemispherical electron analyzer. The calcined samples were pressed into small stainless-steel cylinders and outgassed at 10^{-5} mbar for 1 h before they were moved into the analysis chamber. The residual pressure in the ion-pumped analysis chamber was maintained below 7×10^{-9} Torr during data acquisition. *In situ* pretreatments in hydrogen were carried out at 673 K. Energy regions of the photoelectrons were scanned at a pass energy of 20 eV. Each spectral region was scanned for a number of times to obtain good signal to noise ratios. Peak intensities were estimated by calculating the integral of each peak after subtraction of the S-shaped background and fitting to a curve mixed of Lorenztian and Gaussian lines of variable proportion. Although surface charging was observed for all the samples, accurate binding energies (BE) (± 0.2 eV) could be determined by charge reference to the C 1*s* peak at 284.9 eV.

Activity Measurements

Catalytic tests for hydrogenation of styrene were carried out at atmospheric pressure in an automatic microcatalytic flow reactor and reaction temperature of 363 K. Before introducing the reactant, the samples (0.022 g) were reduced in hydrogen flow (80 ml min^{-1}) at 773 K for 1 h. Then the reactor was purged in a $H_2 : N_2 = 50 : 30$ flow while the temperature was lowered to reaction temperature. The hydrogen/styrene molar ratio was 8.6 with a styrene flow of 0.015 mol h^{-1}. The reaction was carried out at contact time (W/F) of 1.5 g h mol^{-1} and studied over periods of 120 min. The catalysts were pelleted and sieved in the mesh range 0.50–0.42 mm. Tests were made to ensure that the reaction was not subjected to diffusion limitations. Using catalysts sieved in the range 0.84–0.59 mm, results were reproducible within experimental error, indicating that for a gas flow rate of 80 ml min^{-1} diffusion limitation on the reaction rate may be excluded. The products and reactant were analyzed by an on-line Konik 3000 gas chromatograph fitted with a flame ionization detector and a 15% diethylene glycol succinate on Chromosorb W column at 368 K. Selectivity was de-

fined as: 100 × (number of moles of ethylbenzene/number of moles of styrene converted).

RESULTS

Catalyst Characterization

Textural properties. Variation of the BET surface areas of the H_2-reduced samples with lanthanum content is shown in Table 1. For La-modified sepiolite supports, the surface areas markedly decrease with increasing La content. According to previous observation (9), it is likely that the large diameter of La^{3+} ions does not allow La^{3+} to diffuse into the micropore channels of the needle-shaped silicate particles of the support. This fact suggests that in the sepiolite-containing lanthana the oxide may stay on the sepiolite surface. In favor of this argument is the rather low concentration level of lanthanum retained in the final catalyst, because some dissolution of dispersed lanthanum phase occurs during the last impregnation step with nickel nitrate. BET area of Ni/sep catalyst is quite similar to that of the sepiolite substrate. However, BET areas decrease markedly with increasing La loading in both *x*NiLa and Ni*x*La catalysts series. For the Ni deposited onto the La-modified substrates (Ni*x*La series), this decrease represents 25% for the Ni2.3La sample and reaches 33% for its Ni7.1La counterpart. The trend is different for the *x*LaNi catalyst series in which incorporation of La onto Ni-impregnated support leads to a larger decrease in surface area within the catalyst series than for the parent Ni*x*La series. It decreases by only 1% for the 2.3LaNi sample while it drops by 41% for the 8.7LaNi counterpart.

TABLE 1

Catalyst Characteristics and Catalytic Behavior

Catalyst	Ni (%)	S_{BET}[a] ($m^2\ g^{-1}$)	Activity[b] (mol h^{-1} exposed Ni)	Selectivity (%)
Sep	—	143	—	—
2.7La	—	109	—	—
5.0La	—	94	—	—
8.6La	—	84	—	—
Ni/Sep	5.3	138	17.5	99.9
2.3LaNi	5.1	136	3.5	100.0
3.7LaNi	4.6	102	3.4	100.0
8.7LaNi	4.4	82	2.4	100.0
Ni2.3La	4.3	103	0.5	100.0
Ni3.5La	4.7	105	12.2	99.9
Ni7.1La	4.5	93	24.0	99.6

[a] Reduced catalysts.
[b] At 120 min on stream.

Temperature-programmed reduction. Temperature-programmed reduction profiles of *x*LaNi and Ni*x*La catalyst series are displayed in Figs. 1A and 1B, respectively. For the sake of comparison, the reduction profiles of the unpromoted Ni/sep (profile b) and the bare sepiolite substrate (profile a) are included in both figures. All these profiles exhibit a principal peak centered ca. 850 K with shoulders more or less pronounced in the two high- and low-temperature winds. A very small and well-defined peak at ca. 1000 K and a broader and intense one close to 1080 K were also observed in all catalysts. As these two latter peaks are also detected in the bare sepiolite, although with less intensity, they likely arise from the reduction of Fe^{3+} impurities (0.36 wt%) present in the silicate substrate. From the catalytic point of view, the most important differences in both catalyst series lie in the low-temperature region of the principal TPR peak. Comparison of b–e curves in Fig. 1A reveals that Ni-reduction starts at ca. 720 K, irrespective of the presence of La, with a small shoulder centered at ca. 750 K. Although the intensity of this shoulder is somewhat lower for the unpromoted catalyst (curve b), it does not change to a significant extent within the three La-promoted catalysts (curves c–e).

The TPR profiles of Ni*x*La catalyst series in the temperature region below the most intense peak of reduction (720–850 K) is substantially different from that of the *x*LaNi counterparts (Fig. 1B, curves c–e). The shoulder placed in this region is clearly more intense in the Ni*x*La catalyst series than in the parent *x*LaNi samples. As the Ni metallic phase is easier formed on the reduction of Ni^{2+} ions in Ni*x*La, and this is involved in hydrogenation, it appears that these systems are the most promising candidates for styrene hydrogenation. This working hypothesis will then be confirmed in the section of activity results.

Kinetics of reduction. The kinetics of reduction of Ni^{2+} ions is a useful technique to reveal the strength of Ni^{2+}–substrate interaction and how this interaction is altered by the methods of catalyst preparation. Figure 2 displays the kinetic curves of H_2-reduction at 773 K of the unpromoted Ni/sep sample (curve a) and the 7.1LaNi (curve b) and Ni8.7La (curve c) promoted counterparts. It is emphasized in this point that the temperature of 773 K was selected according to the above TPR profiles, at which the rate of reduction is reasonably high. As can be seen, the degree of reduction of Ni^{2+} ions strongly depends on the method of nickel and lanthanum incorporation. At a given time of reduction, the extent of Ni reduction of the unpromoted Ni/sep is substantially higher than that of the promoted Ni8.7La catalyst but much lower, particularly at times below 60 min, than that of its Ni7.1La counterpart prepared by reverse impregnation. A dashed line, parallel to the *X*-axis at $\alpha = 1$, has also been included in this figure to account for the stoichiometric reduction of Ni^{2+} ions to metallic Ni. The trend of the kinetic curves at short times of reduction

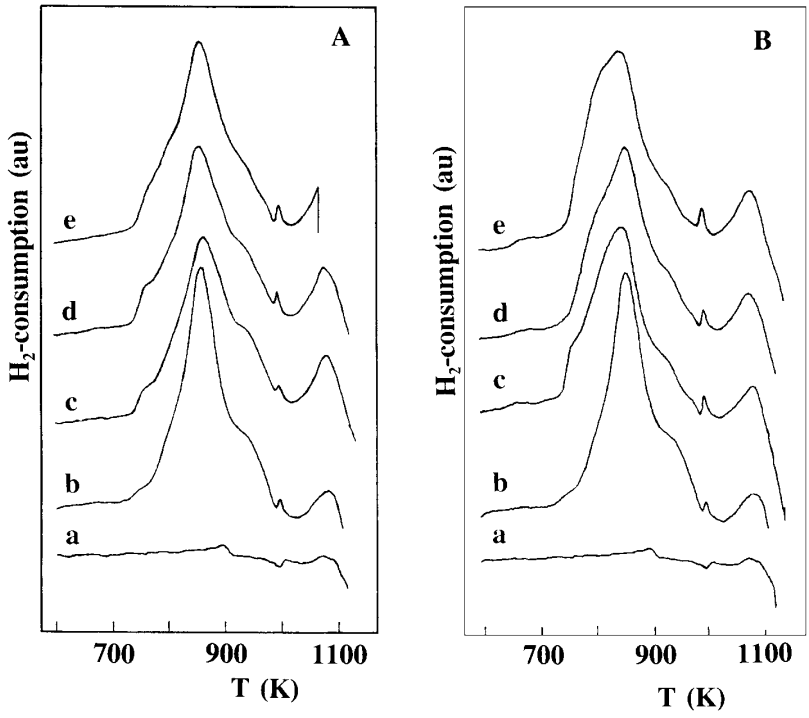

FIG. 1. Temperature-programmed reduction profiles of *x*LaNi (A): (c) 2.3LaNi, (d) 3.7LaNi, (e) 8.7LaNi; and of Ni*x*La catalyst series (B): (c) Ni2.3La, (d) Ni.3.5La, (e) Ni7.1La. For the sake of comparison, the profiles of sepiolite substrate (a), and of Ni/sep (b) have been included in both figures.

is also valid at reduction degree close to equilibrium. For instance, while a reduction time of 180 min is enough to reach equilibrium reduction in catalysts Ni7.1La, reduction times as long as 500 and 720 min are required for the completion of Ni^{2+} reduction in catalysts Ni/sep and 8.7LaNi, respectively. Moreover, considering the quite similar shape of these curves for catalysts Ni/sep and 8.7LaNi it can be inferred that the interaction of Ni^{2+} ions with the silicate substrate is essentially the same (this will then be confirmed by the XP spectra of reduced catalysts). On the contrary,

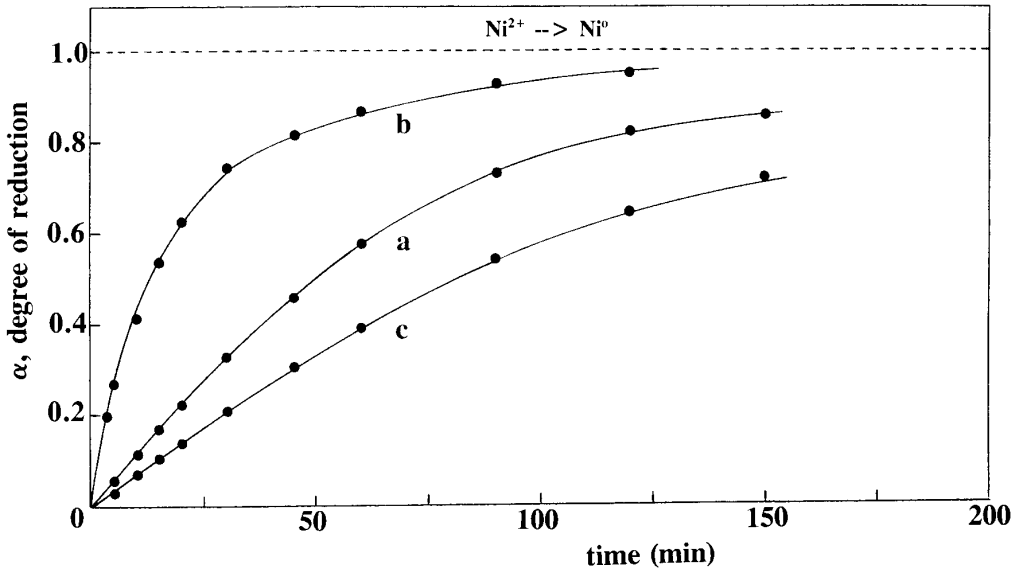

FIG. 2. Kinetic curves of H_2-reduction under isothermal conditions (773 K) of three representative catalysts: (a) Ni/sep; (b) Ni7.1La; and (c) 8.7LaNi. Dashed line represents the stoichiometric reduction of nickel oxide to the metal.

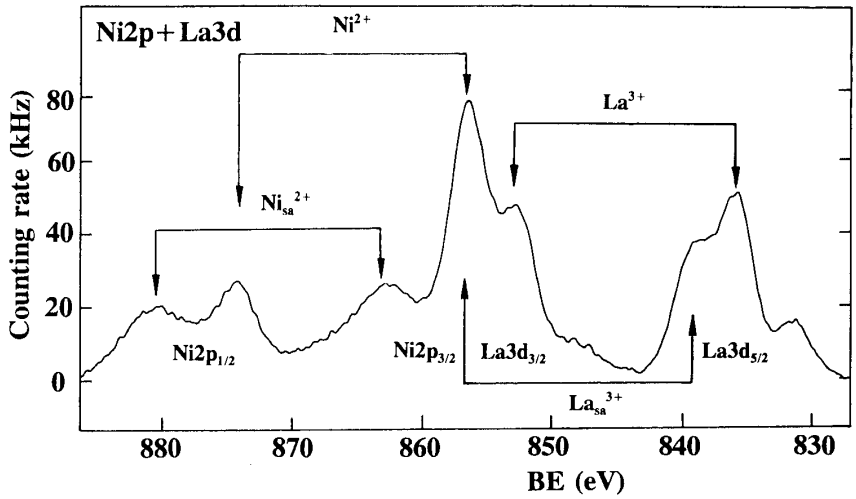

FIG. 3. Photoelectron spectrum in the Ni 2*p*–La 3*d* binding energy region of a representative Ni3.5La catalyst. The spin-orbit splitting and the high binding energy satellites of the principal peaks for both Ni^{2+} and La^{3+} ions are marked by arrows.

the surface structure of Ni^{2+} ions deposited in a second step on a lanthana-modified substrate appears to be completely different.

XPS analysis. The most intense Ni $2p_{3/2}$ peak, which appears at a binding energy about 856.7 eV, is characteristic of Ni^{2+} ions in an oxygen environment (14). This peak is accompanied by a broader one due to shake-up processes located at ca. 6 eV in the high-binding-energy side. This peak is the fingerprint of Ni^{2+} species and can be used to distinguish Ni^{2+} from Ni^0 species. However, the Ni $2p_{3/2}$ profile is complicated by the simultaneous presence of La in both *x*LaNi and Ni*x*La catalyst series, which displays its La $3d_{3/2}$ peak at ca. 4 eV lower BE. Another complication comes from the fact that the closed-shell La^{3+} ion shows its La $3d_{5/2}$ and La $3d_{3/2}$ peaks split by 4.3 eV in two components, which has been assigned to transfer of an oxygen-centered electron to the empty 4*f* shell accompanying the ionization process (15). Accordingly, the higher BE contribution of the La $3d_{3/2}$ peak overlaps with the Ni $2p_{3/2}$ peak (Fig. 3). This overlapping may mask not only the accurate measure of the BE of Ni^{2+} ions but also the presence of Ni^0 in the H_2-reduced catalysts, which is placed in between the two split La $3d_{3/2}$ peaks. To overcome this complication, the Ni $2p_{3/2}$ + La $3d_{3/2}$ energy region was fitted to six components: shake-up satellite line of unreduced Ni^{2+} ions at ca. 863.2 eV, Ni $2p_{3/2}$ principal peak of unreduced Ni^{2+} ions at ca. 857.0 eV, the split La $3d_{3/2}$ peaks at ca. 852.6–856.7 eV, Ni $2p_{3/2}$ line of metallic Ni at ca. 853.5 eV, and the Mg$K\alpha_{3,4}$ satellite of Ni $2p_{3/2}$ and La $3d_{3/2}$ lines. Because no monochromator was used in the X-ray exciting source, this latter line arises from the photoelectrons excited by the Mg$K\alpha_{3,4}$ component. The procedure appears quite accurate as the estimated error in duplicate experiments did not exceed 10%. All these features are illustrated in the XP spectra of H_2-reduced catalysts (Figs. 4A and 4B).

The binding energies of La $3d_{5/2}$ core electrons for La-modified supports, observed at 835.2–835.4 eV, are similar to that observed for dispersed lanthanum on γ-Al_2O_3 (16) and higher than that measured for $La(OH)_3$ (834.8 eV) and La_2O_3 (833.5 eV) (11). Alvero *et al.* (17) attributed the higher-binding-energy species of 835.5 eV to the presence of deficiently coordinated La^{3+} ions on the surface. A La $3d_{5/2}$ binding energy of 836.1 eV was observed by Ledford *et al.* (11) for La/alumina. The La $3d_{5/2}$ binding energies for both series of oxidic and reduced catalysts observed in the range 834.9–835.4 eV are identical to that measured on La/sep series and do not vary with La loading, within experimental error. Ledford *et al.* (11) found a decrease in La $3d_{5/2}$ binding energies measured for reduced CoLa/alumina catalysts from 836.0 to 835.3 eV with increasing La content due to formation of La_2O_3 phase. Incorporation of nickel does not affect the La $3d_{5/2}$ binding energies measured for *x*LaNi catalyst series.

The Ni $2p_{3/2}$ binding energies at ca. 857 eV for oxidic and reduced catalysts (Table 2) characterize the unreduced Ni^{2+} species. The curve synthesis procedure employed gave a less intense contribution at ca. 3.2–3.7 eV lower BE, which is due to metallic Ni. For the sake of comparison, this contribution is overshadowed in all the spectra. The percentage of this peak to the whole area is higher for Ni*x*La than for *x*LaNi series (Figs. 4A and 4B, last column Table 2), although they do not change within each catalyst series. This trend is in good agreement with the kinetic curves of reduction in Fig. 2, although the absolute reduction degree of Ni does not match. These differences may be likely due to differences in H_2 partial pressure during reduction in kinetic experiments by microgravimetry and *in situ* pretreatment within the pretreatment chamber of XPS spectrometer.

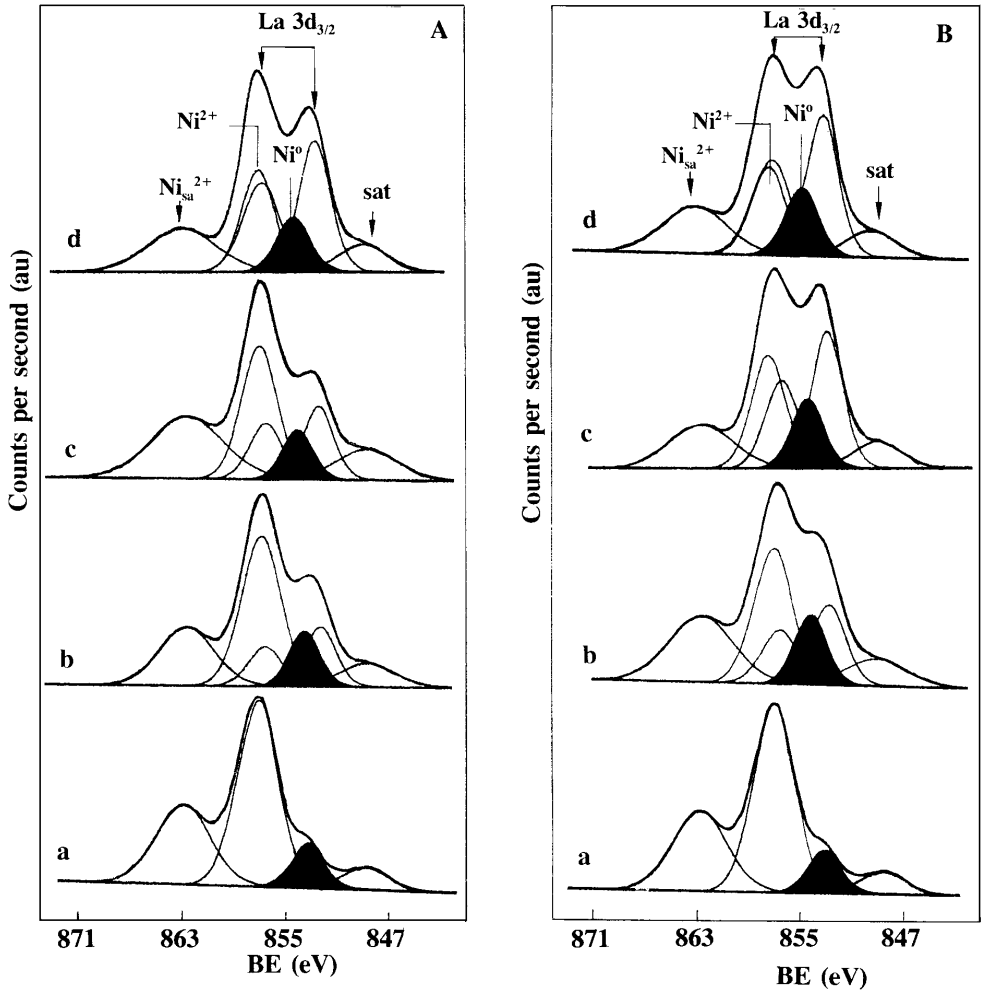

FIG. 4. Photoelectron spectra in the Ni $2p_{3/2}$ + La $3d_{3/2}$ energy region of the *in situ* H_2-reduced catalysts series *x*LaNi (A): (a) Ni/sep, (b) 2.3LaNi, (c) 3.7LaNi, (d) 8.7LaNi; and catalysts series *x*NiLa (B): (a) Ni/sep, (b) Ni2.3La, (c) Ni3.5La, (d) Ni7.1La.

To determine the nature of the distribution of lanthanum phase in the oxidic catalysts and La-modified supports, the La/Si XPS intensity ratio was calculated from the integrated peak intensities. From the plot of these values against lanthanum loading (Fig. 5), it is evident that the lanthanum is better dispersed on the La/sep samples than on the *x*LaNi catalyst series. The similar shape of both lines, although with higher La/Si XPS intensity ratios in the Ni-free samples, suggests that lanthana is distributed in a similar manner in La/sep and *x*LaNi series. These lanthana species seems to be highly dispersed in both systems as no XRD patterns of crystalline lanthana could be recorded. These observations are consistent with the findings of other workers (11, 16, 18), who observed that at low and high loadings lanthanum was present in a dispersed phase with a low coordination of La^{3+} ions and the high BE of La $3d_{5/2}$ at 835 eV resulted only from the dispersed phase but not from crystalline structures. In addition, it has been found (11) that the La/Ni XPS intensity ratios measured for La/alumina samples were approximately 80% of the theoretical value predicted by monolayer dispersion and lanthanum binding energy is independent of loading as long as the lanthanum remains in a dispersed phase. The behavior is quite different for Ni*x*La series. The much higher La/Si XPS intensity ratios found for the Ni2.3La and Ni3.5La catalysts indicate that La distribution becomes altered in the second impregnation step. This is likely due to partial redisolution of deposited lanthana under the low-impregnating pH of the Ni nitrate solution followed by precipitation in the drying steps.

To obtain information about the effect of reduction on the distribution of nickel and lanthanum species, the Ni(La)/Si intensity ratio measured for reduced Ni*x*La and *x*LaNi catalysts is plotted versus the same ratio measured for calcined samples (Fig. 6). From this figure it is clear that the effect of La incorporation on the Ni-reduction depends on the method of preparation. While in *x*LaNi series the degree of reduction of Ni is similar to that of Ni/sep (see last column in Table 2), there is an enhancement in reduction of

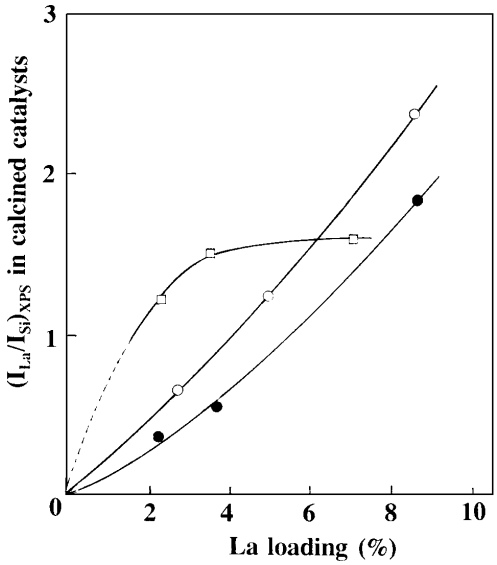

FIG. 5. XPS intensity ratios I_{La}/I_{Si} for calcined catalysts as a function of lanthanum loading for different catalyst series: *x*La/sep (○); Ni*x*La (□); and *x*LaNi (■).

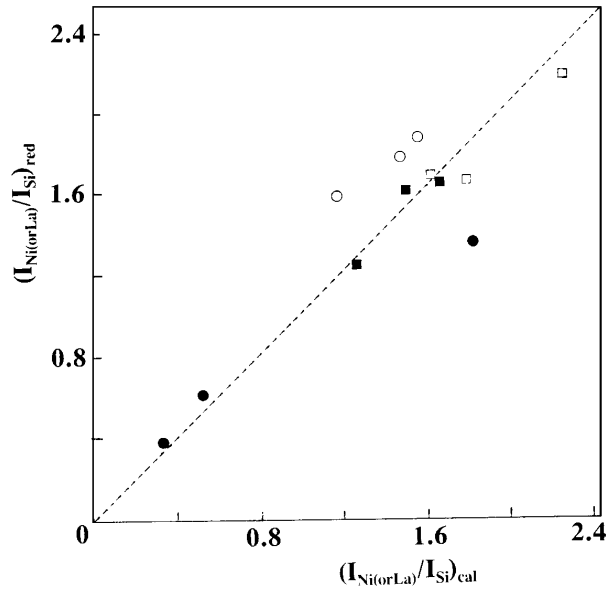

FIG. 6. XPS intensity ratio $I_{Ni(La)}/I_{Si}$ for hydrogen-reduced catalysts as a function of the same ratio $I_{Ni(La)}/I_{Si}$ for calcined catalysts: Ni*x*La series (La (○) and Ni (□)); *x*LaNi series (La (•) and Ni (■)).

Ni*x*La catalyst series. Similarly, the La/Si XPS intensity ratio of Ni*x*La series increases substantially in reduced catalysts. The situation is different for the *x*LaNi series. The La/Si XPS intensity ratios are similar for lower La loadings but decrease drastically in the 8.7LaNi sample, suggesting agglomeration of La_2O_3 phase. In contrast, the increase in La/Si intensity ratio for Ni*x*La series indicates that lanthanum species after reduction are well dispersed on the support.

TABLE 2

Binding Energies (eV) and XPS Intensity Ratios of Calcined and H_2-Reduced La-Promoted Ni/Sepiolite Catalysts

Catalyst	Si 2*p*	La $3d_{5/2}$	Ni $2p_{3/2}$	I_{La}/I_{Si}	I_{Ni}/I_{Si}	Ni^0/Ni_t^b
2.7La	102.4	835.3	—	0.64	—	—
5.0La	102.3	835.4	—	1.25	—	—
8.6La	102.5	835.2	—	2.41	—	—
Ni/Sep	102.3	—	857.4	—	1.74	—
	102.5	—	857.3–853.2[a]	—	1.65	0.09
2.3LaNi	102.5	835.4	857.1	0.34	1.29	—
	102.4	835.3	857.0–853.5[a]	0.37	1.23	0.11
3.7LaNi	102.3	835.2	857.2	0.53	1.70	—
	102.4	835.4	857.2–853.4[a]	0.60	1.63	0.09
8.7LaNi	102.4	835.2	857.1	1.85	1.53	—
	102.3	835.2	857.2–853.2[a]	1.33	1.60	0.11
Ni2.3La	102.5	834.9	857.0	1.19	1.84	—
	102.4	835.3	856.9–853.9[a]	1.57	1.64	0.13
Ni3.5La	102.4	835.3	857.0	1.51	2.31	—
	102.5	835.3	857.0–853.8[a]	1.75	2.17	0.13
Ni7.1La	102.6	835.4	856.9	1.59	1.65	—
	102.5	835.2	856.8–854.0[a]	1.86	1.66	0.13

[a] This peak corresponds to reduced nickel.
[b] Estimated error in this calculation is 8%.

Considering the low reduction levels of Ni in the last column of Table 2, the relative high Ni/Si intensity ratio for Ni*x*La series after reduction compared to that for *x*LaNi samples suggests that a possible interaction between La and Ni may suppress the agglomeration of the nickel species during the preparation. Barrault *et al.* (19) proposed that the suppression of H_2 chemisorption on CoLa catalysts supported on carbon may be due to migration of LaO_x moieties to the surface of metal particles. Ledford *et al.* (11) and Zhang *et al.* (6) attributed the higher dispersion of Co_2O_3 and NiO in La-promoted catalysts to formation of La–Co and La–Ni mixed oxides, respectively, or NiO particles separated by La_2O_3. In our case, some decoration of nickel species by La may occur during nickel impregnation. The formation of a LaO_x oxide on Ni particles during reduction is unlikely in the Ni*x*La catalyst series. The observed SMSI phenomenon for La-promoted Pd/SiO_2 catalysts (2) must be excluded in our case, since this effect is revealed at high-temperature reduction. Most probably, decoration of the nickel species by La occurred due to redissolution of La_2O_3 (3) during $Ni(NO_3)_2$ impregnation.

IR spectra. Figure 7 shows infrared spectra of adsorbed carbon monoxide on reduced sepiolite-supported nickel and nickel–lanthanum catalysts. In agreement with our previous IR data on nickel/sepiolite catalysts (12) and literature measurements (19–24), two adsorption states of CO in the region 2100–1850 cm^{-1} are observed: a linear form above 2000 cm^{-1} (2090–2080 and 2016–2012 cm^{-1} and a bridged one below 2000 cm^{-1} (1960–1956 and 1940 cm^{-1}). These bands are assigned to CO adsorption on reduced Ni

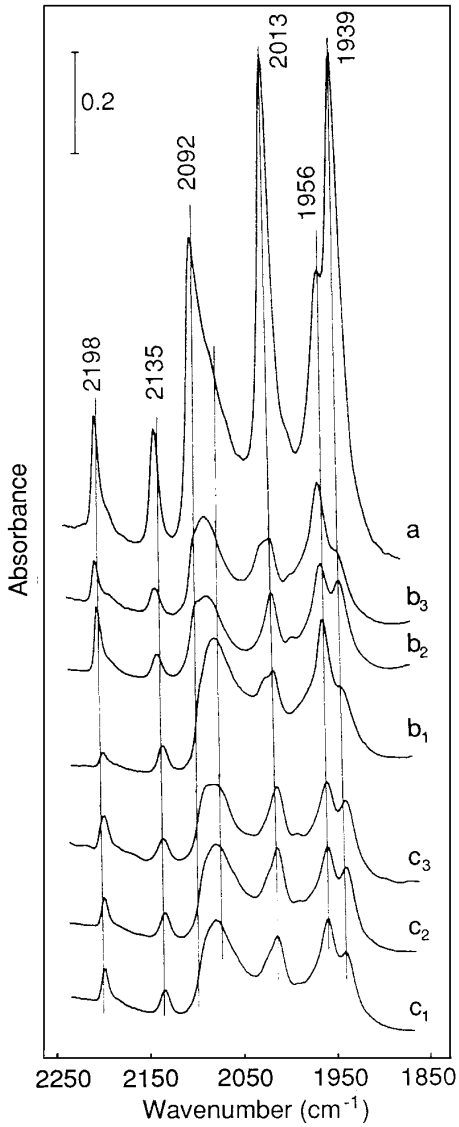

FIG. 7. IR spectra of carbon monoxide adsorption at room temperature on prereduced catalysts at 673 K: Ni/sep (a), Ni2.3La (b_1), Ni3.5La (b_2), Ni7.1La (b_3), 2.3LaNi (c_1), 3.7LaNi (c_2) and 8.7LaNi (c_3).

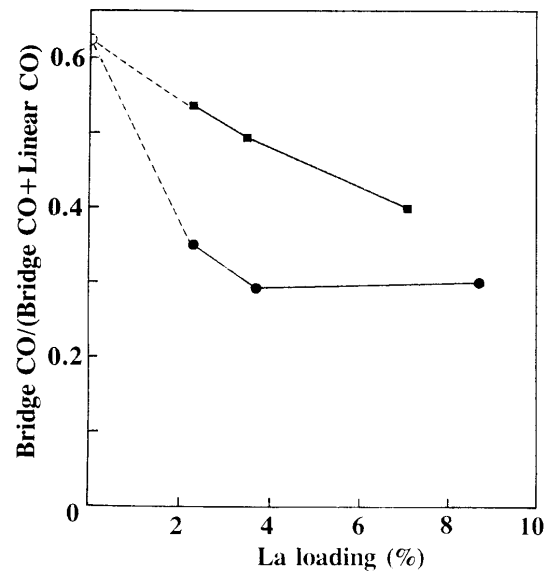

FIG. 8. Ratios of bridged adsorbed CO to the sum of linear and bridged adsorbed CO as a function of lanthanum loading for NixLa (■) and xLaNi catalyst series (●).

sites and are referred to as L1, L2, B1, and B2 in order of decreasing vibrational frequency. The bands at 2198 and 2135 cm^{-1}, indicative of incompletely reduced nickel species, are attributed to CO adsorbed on Ni^{2+} and Ni^{+} ions, respectively. The unreduced Ni^{2+} species could arise from the presence of oxidic nickel species, which are stabilized on the catalyst surface against reduction conditions (12, 25).

The ratio of integrated optical densities of bridged to the sum of linear (L2 band) and bridged species as a function of La loading, displayed in Fig. 8, can be taken as a measure of the relative abundance the observed species (22). It is evident from Fig. 8 that the La promotion causes preferential suppression of bridge-bonded CO species relative to linearly bonded ones for xLaNi series with increasing La loading. With regard to reduced nickel sites, the bands attributed to bridged species always appeared as the most intense feature for NixLa series. Another distinguishing feature of CO adsorption on La-modified catalysts is the increase in the relative intensity of the band near 2080 cm^{-1} compared to bands at 2016 cm^{-1} (this contrasts with the Ni/sep catalyst) and simultaneously its shift to higher wavenumbers (to about 2090 cm^{-1}) with increasing La content, indicative of a low level of reduction and higher dispersion (22).

A decrease in CO adsorption with increasing La content has also been reported for Rh–La_2O_3/SiO_2 (26) catalysts. This was explained by a partial coverage of the Rh particles resulting from the dissolution of La_2O_3 when impregnating with $Rh(NO_3)_3$ solution. The higher H/Rh chemisorption values as regards CO/Rh ones were explained by spillover of H atoms to the La_2O_3 and to reduction of the promoter oxide to LaO_x. The observed suppression of CO adsorption on La-promoted Pd/SiO_2 catalysts by Hicks *et al.* (27) was attributed to patches of partially reduced support material LaO_x, transferred to the surface of the Pd crystallites during catalyst preparation, leading to weakening in the σ-bond component of the Pd–CO bond. The direction of charge transfer between the LaO_x patches and the Pd was derived from the shift to lower frequency of bridge-bonded species. However, in our case neither infrared spectra of CO adsorbed nor XPS measurements have shown evidence for electronic effects. In contrast to this, Schultz *et al.* (28) observed an increase in H_2 and CO chemisorption with increasing La content in Rh/SiO_2 system. They demonstrated that the promotion effect of La on Rh/SiO_2 catalyst consisted of the prevention of sintering of Rh crystallites, rather

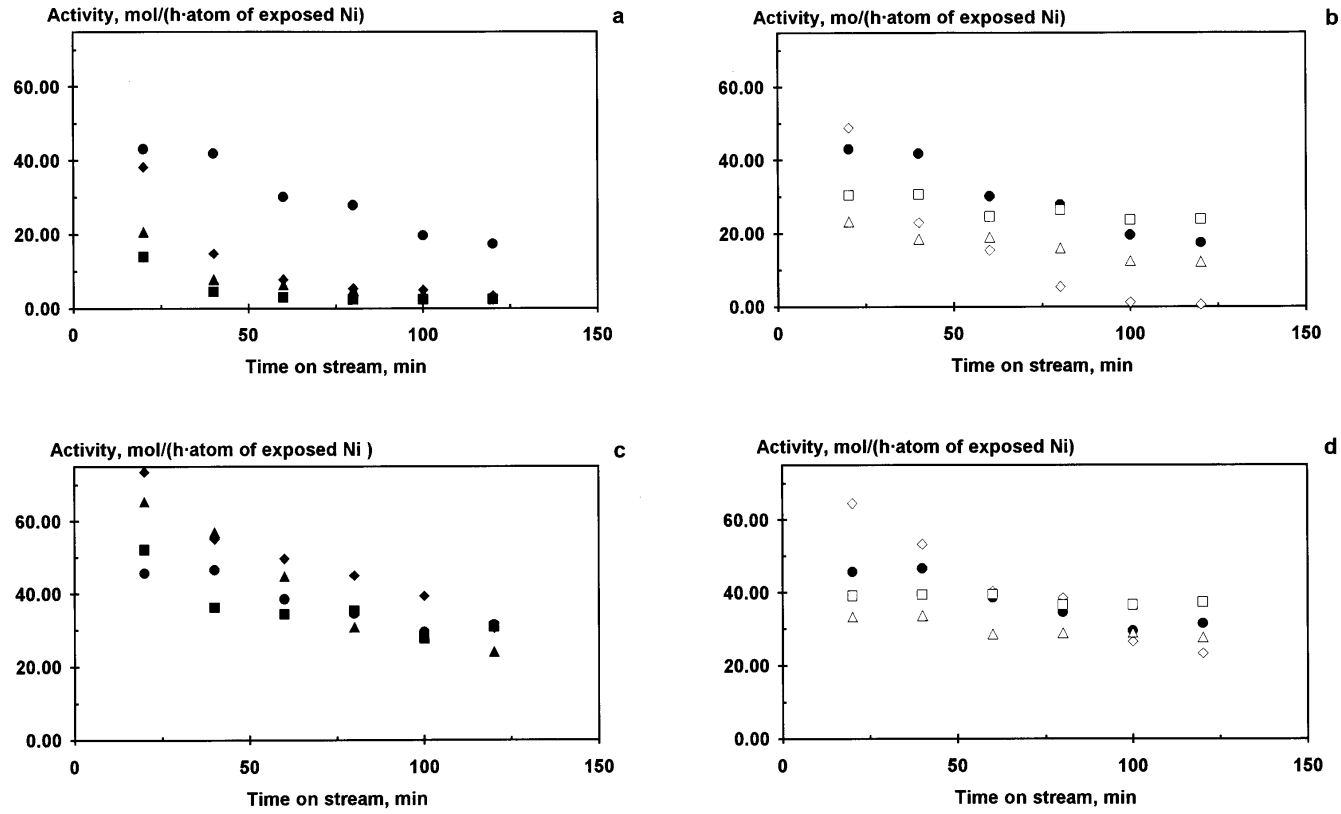

FIG. 9. Specific activity of styrene hydrogenation with time on stream for *x*LaNi series (a); Ni/sep (●), 2.3LaNi (⧫), 3.7LaNi (▲), 8.7LaNi (■), and Ni*x*La series (b): Ni2.3La (◇), Ni3.5La (△), and Ni7.1La (□). Specific activities of styrene hydrogenation for *x*LaNi (c) and Ni*x*La (d) series after regeneration in hydrogen. Symbols are the same as above.

than their covering by LaO_x moieties in the reduced state of the catalyst as has been explained by other authors (2, 19).

The CO adsorption results indicate that the exposed Ni atoms on the catalyst surface could be grouped in two categories: Ni atoms adsorbing CO and Ni atoms partially covered by the promoter oxide, which do not adsorb CO. The proportion of Ni surface atoms in which CO adsorption is suppressed increases with increasing La loading in the catalyst (Fig. 8).

Styrene hydrogenation. The specific activities of the catalysts in styrene hydrogenation, expressed by the number of styrene molecules coverted per hour and exposed Ni atom and their selectivities to etylbenzene at 120 min on stream, are summarized in Table 1. The atoms of exposed Ni were calculated from XPS Ni/Si ratios, but by considering only the fraction of reduced nickel (Ni^0). These activities have been obtained under experimental conditions that approach differential conditions, e.g., styrene conversions below 30%. A fast activity increase with increasing La content was observed in Ni*x*La series, whereas the trend is opposite and much more smoothed for *x*LaNi series. For Ni*x*La catalysts a maximum in activity is observed for a 7.1% La, which is 37% higher than for the unpromoted Ni/sep sample. Moreover, activity data for catalysts with La loadings above 2.3% are much higher in *x*LaNi series. On the contrary, selectivity to ethylbenzene is complete for *x*LaNi catalysts and almost complete for the unpromoted Ni/sep and Ni*x*La catalysts. Apart from ethylbenzene, which is the major hydrogenated product, very small amounts of ethylcyclohexane are also detected for Ni/sep and 3.7LaNi and 8.7LaNi catalysts. Since the nickel content does not significantly change for both catalysts series, the differences in their catalytic behavior must be related to the differences in catalyst morphology and structure induced by the two preparation methods.

The effects of lanthanum content, preparation method and regeneration on the styrene hydrogenation can be revealed by plotting the specific activity as a function of the time on stream for both catalyst series (Ni*x*La and *x*LaNi). As stated above, hydrogenation activity decreases with increasing La content for *x*LaNi catalysts (Fig. 9a) at short times on stream, but these differences are smoothed at longer times. The common feature of all these curves is that catalysts deactivate, but the extent of deactivation is different from that of the unpromoted Ni/sep catalyst: while after 120 min on stream activity is only reduced to ca. 50% in the Ni/sep sample it is practically inhibited in *x*LaNi

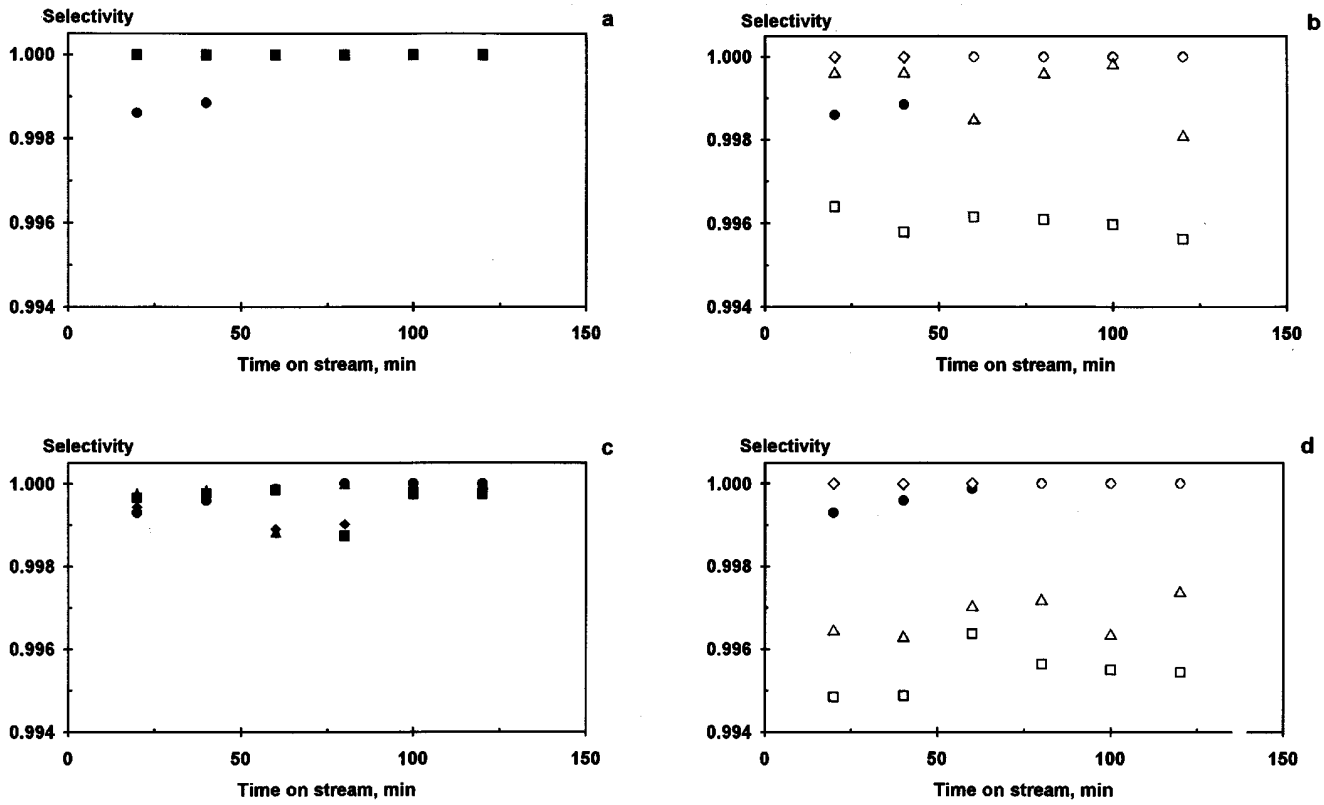

FIG. 10. Selectivities to ethylbenzene with time on stream for *x*LaNi series (a): Ni/sep (•), 2.3LaNi (♦), 3.7LaNi (▲), 8.7LaNi (■), and Ni*x*La series (b): Ni2.3La (◇), Ni3.5La (△), and Ni7.1La (□). Selectivities for *x*LaNi (c) and Ni*x*La (d) series after regeneration in hydrogen. Symbols are the same as above.

catalysts. Irrespective of these changes, selectivity to ethylbenzene is complete for all *x*LaNi catalyst and times on stream (Fig. 10a).

Activity profiles of catalyst series Ni*x*La are quite different from that of the parent *x*LaNi series. While the initial activity of the Ni2.3La catalyst is somewhat above that of the unpromoted sample and becomes completely deactivated at 120 min on stream (Fig. 9b), the Ni3.5La and Ni7.1La catalysts display a less marked deactivation. Particularly, the activity of Ni7.1La sample at 120 min on stream process becomes higher than that of its unpromoted Ni/sep counterpart. Selectivities to ethylbenzene are very high along this catalyst series (Fig. 10b), with some irrelevant decrease until ca. 0.996 for the Ni7.1La catalyst.

As catalyst deactivation under the very mild reaction conditions used in the present work is expected to be due to formation of polymers on Ni crystallites, all the used catalysts for 120 min on stream were reduced again at 773 K for 1 h. Activity patterns for regenerated *x*LaNi and Ni*x*La catalyst series are shown in Figs. 9c and 9d, respectively. For both catalyst series activity not only is recovered but also overpasses the level of fresh catalysts. Moreover, deactivation is slower in both series. For regenerated Ni*x*La catalyst series activity becomes more and more sustained with increasing La loading while retaining a high level. Note that the activity decrease is important for the Ni2.3La, moderate for the Ni3.5La, and irrelevant for the Ni7.1La sample (Fig. 9d). The tendencies are less clear for the *x*LaNi catalyst series. Selectivities to ethylbenzene are practically 100% in *x*LaNi catalysts (Fig. 10c), with minor deviations in Ni*x*La catalyst, particularly at high La loadings, although they are maintained above 0.995% (Fig. 10d).

DISCUSSION

The kinetics of reduction (Fig. 2)and XPS data (Figs. 4A, 4B, and 5) indicate clearly that Ni^{2+} ions interact strongly with the sepiolite substrate in *x*LaNi samples and to a lesser extent in Ni*x*La series. On the other hand, the IR spectra of CO adsorbed on the reduced catalysts (Fig. 7) demonstrate that the promotion of Ni/sepiolite catalyst with lanthana results in a change in the distribution of CO-adsorbed structures. A remarkable feature of the active sites induced by the presence of La in the catalysts is that the adsorption of CO on both catalyst series is not so strong as for the La-free catalyst counterpart. Similar observation has already been reported for La-promoted Ni and Pd catalysts (27, 29). One of the principal differences among the samples is

the intensity distribution of B1 and B2 bands. The change in the relative intensities of these two bands is clearly visible by comparing the spectra of Ni/sep and La-promoted catalysts on the one hand and the spectra of Ni*x*La series relative to *x*LaNi series on the other hand. While B1 band appears as a shoulder for the Ni/sep sample, incorporation of La significantly affects the suppression of B2 band relative to B1, this being more pronounced for Ni2.3La and 2.3LaNi samples. The infrared study of CO adsorption on nickel crystallites revealed that the frequencies of the B1 and B2 bands are very close to frequencies of the bands for bridged-bonded CO to Ni(100) and Ni(111) surfaces, respectively (12). Thus, the distribution of B1 and B2 adsorption sites will be connected with a change in the morphology of the exposed Ni particles. The increase in the intensity of the B1 band after La promotion suggests that reconstruction of bridge-bonded species occurs via formation of Ni(100) surfaces. Another important conclusion derived from the data in Fig. 8 is that CO can be adsorbed in a linear form on Ni atoms, which are in contact with oxidic phase. Thus, the interpretation for a decrease of the bridged form and relative higher concentration of unreduced nickel species gives an indication that lanthanum is deposited on the nickel particles, leading to a decrease in the probability to have adjacent nickel atoms on the surface, as suggested by Primet *et al.* (23).

According to previous studies (2, 19), the sites responsible for hydrogenation might involve lanthanum species on the surface of large metal particles, even though the structural information described above showed that La incorporation has little effect on the chemical state of nickel sites. Barrault *et al.* (19) showed that La-promotion effect on carbon-supported cobalt catalysts in CO hydrogenation is attributed to formation of active sites on metal particles. Ledford *et al.* (11) reported that highly dispersed cobalt metal in CoLa/alumina catalysts is not active in CO hydrogenation, while Schultz *et al.* (28) demonstrated that the main role of the lanthanum promoter in the CO hydrogenation is the prevention of sintering of the Rh crystallites. For Ni*x*La series, the La_2O_3 or La^{3+} ions on sepiolite, formed during the first impregnation, maybe also act as adsorption centers for Ni^{2+} ions in the second impregnation with $Ni(NO_3)_2$ and preventing sintering of metallic Ni crystallites during reduction. However, some redistribution of the La_2O_3 phase may occur during the second impregnation with Ni^{2+}. This is confirmed by the unusually high La/Si XPS intensity ratio found in Ni2.3La and Ni3.7La catalysts (Fig. 5). For the Ni7.1La catalyst, not only a larger fraction of the silicate substrate may be covered by La but also the Ni particles deposited on it might well be covered by the La_2O_3 redistributed, thus leading to optimization of the active site.

The catalysts prepared by reverse impregnation (*x*LaNi series) were examined to separate the effects of La addition and Ni dispersion on their catalytic properties. The addition of La after nickel affects the styrene hydrogenation in comparison with unpromoted nickel catalyst. This fact can be due not only to La blocking of the active nickel sites, which are covered to a great extent as revealed by the rapid deactivation of the catalysts with time on stream (Fig. 9a), but also to changes in the environment of the individual Ni atoms in Ni crystallites, as already revealed by the IR spectra of CO. Considering the infrared results, presented in Figs. 7 and 8, deactivation of the catalysts in the high-loading region is deemed to be a consequence of lanthanum coverage on the catalytically active Ni surface. Finally, activity recovered after regeneration in hydrogen of both *x*LaNi and Ni*x*La catalysts series suggests a reconstruction of the Ni–La_2O_3 interface via formation of Ni(100) surfaces. As this interface is essentially formed on a partially La_2O_3-coated substrate, which minimizes Ni losses through reaction with the silicate substrate, high La loadings have to be used. Consistently, stable catalysts are obtained at the highest La loadings (Ni7.1La).

ACKNOWLEDGMENTS

S. Damyanova is grateful to the Ministerio de Education y Ciencia of Spain for a grant received under the sabbatical program. The authors acknowledge the assistance of Dr. B. Pawelec in recording TPR profiles.

REFERENCES

1. Fleish, T. H., Hicks, R. F., and Bell, A. T., *J. Catal.* **87**, 398 (1984).
2. Rieck, J. S., and Bell, A. T., *J. Catal.* **96**, 88 (1985).
3. Kieffer, R., Kiennemann, A., Rodriguez, M., Bernal, S., and Rodriguez, Izquierdo, J. M., *Appl. Catal.* **42**, 77 (1988).
4. Baker, B. G., and Clark, N. J., *Stud. Surf. Sci. Catal.* **31**, 455 (1987).
5. Imamura, H., Yoshimura, K., Hiranaka, Sh., Sakata, Y., and Tsuchiya, S., *J. Chem. Soc. Faraday Trans.* **87**, 2805 (1991).
6. Zhang, L., Lin, J., and Chen, Y., *J. Chem. Soc. Faraday Trans.* **88**, 497 (1992).
7. Imamura, H., Konishi, T., Sakata, Y., and Tsuchiya, S., *Bull. Chem. Soc. Jpn.* **65**, 244 (1992).
8. Inui, T., Funabiki, M., Suehiro, M., and Serume, T., *J. Chem. Soc. Faraday Trans.* **71**, 787 (1979).
9. Schaper, H., Doesburg, E. B. M., Korte, P. H. M., and Reijen, L. L., *Appl. Catal.* **14**, 371 (1985).
10. Schaper, H., Amesz, D. J., Doesburg, E. B. M., and Reijen,, L. L., *Appl. Catal.* **9**, 129 (1984).
11. Ledford, J. S., Houalla, M., Proctor, A., and Hercules, D. M., *J. Phys. Chem.* **93**, 6770 (1989).
12. Anderson, J. A., Daza, L., Fierro, J. L. G., and Rodrigo, M. T., *J. Chem. Soc. Faraday Trans.* **89**, 3651 (1993).
13. Anderson, J. A., Daza, L., Damyanova, S., Fierro, J. L. G., and Rodrigo, M. T., *Appl. Catal. A: General* **113**, 75 (1994).
14. Briggs, D., and Seah, M. P., "Practical Surface Analysis: Auger and X-ray Photoelectron Spectroscopy," 2nd ed. Wiley, Chichester/New York, 1990.
15. Jorgensen, C. K., and Berthou, H., *Chem. Phys. Lett.* **13**, 186 (1972).

16. Haack, L. P., Peters, C. R., Vriesand, J. E., and Otto, K., *Appl. Catal. A: General* **87**, 103 (1992).
17. Alvero, R., Bernal, A., Carrizosa, I., and Odriozola., J. A., *Inorg. Chim. Acta* **140**, 45 (1987).
18. Jun-Ying, Y., and Swartz, W. E., *Spectrosc. Lett.* **17**, 331 (1984).
19. Barrault, J., Guillemont, A., Achard, J. C., Paul-Boucour, V., and Percheron-Guegan, A., *Appl. Catal.* **21**, 307 (1986).
20. Eischens, R. P., Francis, S. A., and Pliskin, W. A., *J. Phys. Chem.* **60**, 194 (1956).
21. Yates, J. T., and Garland, C. W., *J. Phys. Chem.* **65**, 617 (1961).
22. Peri, J. B., *J. Catal.* **86**, 84 (1984).
23. Primet, M., Dalmon, J. A., and Martin, G. A., *J. Catal.* **46**, 25 (1977).
24. Hardeveld, R., and Hartog, F., *Adv. Catal.* **22**, 75 (1972).
25. Daza, L., Pawelec, B., Anderson, J. A., and Fierro, J. L. G., *Appl. Catal.* **87**, 45 (1992).
26. Gallagher, G., Goodwin, J. G., Chen-Shi, H., and Houalla, M., *J. Catal.* **127**, 719 (1991).
27. Hicks, R. F., Yen, Q., and Bell, A. T., *J. Catal.* **89**, 498 (1984).
28. Schultz, E., Borer, A. L., and Prins, R., *Catal. Lett.* **14**, 279 (1992).
29. Imamura, H., Sugimoto, H., Sakata, Y., and Tsuchiya, S., *J. Catal.* **136**, 271 (1992).